PHYSICAL REVIEW A VOLUME 36, NUMBER 6 SEPTEMBER 15, 1987

Classical and semiclassical approximations for incoherent neutron scattering

E. J. Heller
Departments of Chemistry and Physics, University of Washington, Seattle, Washington 98195

Jeffrey R. Reimers*
Department of Chemistry, B014 University of California San Diego, La Jolla, California 92093

Gerhard Drolshagen
Max-Planck-Institut für Stromungforschung Bunsenstrasse 10, D-3400 Göttingen, West Germany
(Received 2 October 1986)

Recent experience with semiclassical approximations with wave packets make possible a new intuitive basis and new computational tools for incoherent neutron scattering. We review our approach in the context of others which have been proposed for neutron scattering, and we find it advantageous to launch semiclassical approximations from the Schrödinger picture rather than the Heisenberg picture of quantum mechanics. An application to a model for crystalline HCN is given.

I. INTRODUCTION

Since the 1954 Van Hove paper[1] on correlation and response functions, the fundamental basis for the theoretical description of neutron scattering has been a dynamical one. In condensed-matter physics, the starting place for theories of many kinds of spectra has traditionally been in terms of time-dependent correlation functions. In contrast, gas-phase spectroscopy has historically been given a "static" perspective: spectra described in terms of eigenvalues and matrix elements involving eigenfunctions. More recently, progress has been made in understanding and computing gas-phase spectral features in terms of dynamics of the molecules.[2,3] Of special concern here is the context of semiclassical dynamics of wave packets representing nuclear motion of the molecule,[3,4] from which electronic, resonance Raman, and inelastic time-of-flight molecular spectroscopies may be derived. In molecular spectroscopy, the wave-packet techniques have made possible calculation of molecular spectra (specifically electronic and Raman spectra) of polyatomic molecules, at low and high temperatures, without resort to the usual harmonic approximations. Wave packets have given accurate results for highly anharmonic molecules, especially for spectra which are unresolvable due to a very high (or infinite) density of states. Neutron inelastic scattering spectra are of this type, and the success in the molecular world of the new semiclassical wave-packet methods suggests they be explored for possible application to neutron scattering. The present paper does this and we believe a computationally and intuitively useful alternative to the usual formalism is the result. It is our belief that the semiclassical wave packets are a worthwhile addition to the intuitive and computational neutron scattering toolbox.

The usual formulation of neutron scattering employs the Heisenberg picture of quantum mechanics. The Heisenberg picture is a natural starting point for semiclassical approximations, providing the operators have a classical analog. Sometimes, as in the case of electronic and resonance Raman spectroscopies, no classical analog (in the Heisenberg picture) exists, at least not if the Born-Oppenheimer separation of electronic and nuclear motion is presumed. (The Appendix contains a discussion of this issue and the relation of neutron scattering to electronic spectroscopy.) However, working from the Scrhödinger picture, one can obtain a very useful semiclassical method. The method involves propagating time-dependent wave packets along classical trajectories, making them "semiclassical wave packets." This approach, when applied to neutron scattering, is not equivalent to any of the traditional classical or semiclassical methods for simulating neutron scattering, except in the exactly soluble cases (harmonic oscillators, etc.). Even in these cases, the underlying intuition is quite distinct from the usual one derived from the Heisenberg picture.

We pursue the implications of the semiclassical wave-packet picture for neutron scattering, aided by the concise books by Lovesey.[5] The semiclassical wave-packet techniques we use are a combination of the coherent-state formalism,[6] which by itself is too restrictive for our purposes, and semiclassical wave-packet propagation techniques. Recently, Littlejohn has given a very complete and rigorous discussion of semiclassical wave-packet-propagation methods.[7] Also, the present methods are much simpler than a full semiclassical-limit implementation of coherent-state path integrals.[8]

The organization of the paper is as follows. In Sec. II we recall the basic equations for incoherent neutron scattering, including the correlation-function expressions. Merits of two different semiclassical implementations of the correlation functions are discussed. The second of these, namely, a wave-packet picture of semiclassical and quantum dynamics, is augmented in Sec. III. Applications of both methods to the impulse approximation and to scattering from a harmonic solid are developed and contrasted in Sec. IV. A third approach, namely, the Wigner representation with a semiclassical implementa-

tion of the dynamics, is also discussed in the context of harmonic-oscillator scattering. All three methods are, of course, exact for the case of a harmonic oscillator, but all three point the way to the inclusion of anharmonicities in different ways. In Sec. V an application to the anharmonic modes of an HCN molecule embedded in a (static) lattice is given.

II. CORRELATION FUNCTIONS AND THE HEISENBERG VERSUS THE SCHRÖDINGER PICTURES

A. Correlation functions and neutron scattering: the Heisenberg picture

Following the notation of Lovesey,[5] the differential cross section due to incoherent neutron scattering is

$$\frac{d^2\sigma}{d\Omega dE}=N\frac{k'}{k}\frac{\sigma_i}{4\pi}S_i(\mathbf{k},\omega) , \tag{2.1}$$

where N is the number of scatterers, σ_i is the total incoherent cross section, k and k' are the initial and final wave-vector magnitudes of the neutron, $\mathbf{k}$ is the momentum transfer, and $S_i(\mathbf{k},\omega)$ is the response function, or "dynamic structure factor" for neutron scattering. The response function is in turn given in terms of a Fourier transform of a correlation function,

$$S_i(\mathbf{k},\omega)=\frac{1}{2\pi N\hbar}\int_{-\infty}^{\infty}dt e^{-i\omega t}\sum_j Y_{jj}(\mathbf{k},t) , \tag{2.2}$$

where the correlation function $Y_{jj}(\mathbf{k},t)$ is the Fourier transform of the self-pair-correlation function

$$G_s(\mathbf{q},t)=\frac{1}{N}\sum_j\int d\mathbf{q}'\langle\delta(\mathbf{q}-\mathbf{q}'-\hat{\mathbf{q}}_j)\delta[\mathbf{q}'-\hat{\mathbf{q}}_j(t)]\rangle . \tag{2.3}$$

The function $Y_{jj}(\mathbf{k},t)$ may be expressed as

$$\begin{aligned}Y_{jj}(\mathbf{k},t)&=\langle e^{i\mathbf{k}\cdot\hat{\mathbf{q}}_j}e^{i\hat{H}t/\hbar}e^{i\mathbf{k}\cdot\hat{\mathbf{q}}_j}e^{-i\hat{H}t/\hbar}\rangle\\&=\langle e^{-i\mathbf{k}\cdot\hat{\mathbf{q}}_j}e^{i\mathbf{k}\cdot\hat{\mathbf{q}}_j(t)}\rangle ,\end{aligned} \tag{2.4}$$

where the brackets signify an ensemble average. Coherent inelastic neutron scattering involves $Y_{ij}(\mathbf{k},t)$, $i\neq j$. The semiclassical wave-packet methods for incoherent scattering derived below apply to coherent scattering as well.

The Heisenberg operator $\hat{\mathbf{q}}_j(t)$ obeys

$$\begin{aligned}\frac{d\hat{\mathbf{q}}_j(t)}{dt}&=\frac{\partial\hat{H}}{\partial\hat{\mathbf{p}}_j} ,\\\frac{d\hat{\mathbf{p}}_j(t)}{dt}&=-\frac{\partial\hat{H}}{\partial\hat{\mathbf{q}}_j}=-\frac{\partial\hat{V}}{\partial\hat{\mathbf{q}}_j} ,\end{aligned} \tag{2.5}$$

where $\hat{V}$ is the interaction potential for the whole system of particles. The solution of these equations is

$$\begin{aligned}\hat{\mathbf{q}}_j(t)&=e^{i\hat{H}t/\hbar}\hat{\mathbf{q}}_j e^{-i\hat{H}t/\hbar} ,\\\hat{\mathbf{p}}_j(t)&=e^{i\hat{H}t/\hbar}\hat{\mathbf{p}}_j e^{-i\hat{H}t/\hbar} .\end{aligned} \tag{2.6}$$

An interesting alternate form for Eq. (2.4) is

$$\begin{aligned}Y_{jj}(\mathbf{k},t)&=\langle e^{i\hat{H}'_j t/\hbar}e^{-i\hat{H}t/\hbar}\rangle ,\\\hat{H}'_j&=e^{-i\mathbf{k}\cdot\hat{\mathbf{q}}_j}\hat{H}_j e^{i\mathbf{k}\cdot\hat{\mathbf{q}}_j} ,\\&=\hat{H}(\hat{\mathbf{p}}+\hbar\mathbf{k}_j,\hat{\mathbf{q}}) ,\end{aligned} \tag{2.7}$$

and $\hbar\mathbf{k}_j$ is the momentum imparted by the neutron to the jth nucleus. (The notation $\hat{\mathbf{p}}+\hbar\mathbf{k}_j$ is understood to imply the momentum $\hbar\mathbf{k}$ is imparted to the jth particle). We call $\hat{H}'_j$ a momentum-shifted Hamiltonian. Apparently, neutron scattering can be viewed as arising from a correlation function involving two distinct Hamiltonians, related by a momentum shift. Appendix A shows the close connection between incoherent neutron scattering and electronic spectroscopy involving position-shifted potentials.

Equation (2.4) is expressed in the Heisenberg picture and is very suggestive of semiclassical approximation. A primitive classical approximation is obtained simply by letting the operators become their classical analogs, and taking the trace over a classical equilibrium ensemble. Much is lost, however, in such a simple and direct approach. For example, the noncommutation of $\hat{p}$ and $\hat{H}(\hat{p},\hat{q})$ is ignored. It is possible to include some of the effects of noncommutation of $\hat{p}$ and $\hat{H}(\hat{p},\hat{q})$ and obtain an improved classical approximation. This is discussed by Lovesey,[5] and at the end of this section.

B. The Schrödinger picture

There is a different route to a useful semiclassical procedure. We remain in the Schrödinger picture and make a special choice of a quantum-mechanical basis (the coherent states) in which to evaluate the trace involved in computing the ensemble average. The coherent states are then propagated semiclassically. See Ref. 6 for a discussion giving the basic properties of the coherent states and references to several excellent works on this subject. The term "harmonic-oscillator coherent state" has a somewhat more restricted meaning than "Gaussian wave packet" but we shall use them interchangeably. The basic idea of their use in semiclassical contexts is that they can have well-defined positions and momenta (within the limits of the uncertainty principle), and that they follow classical-like trajectories under propagation by smooth Hamiltonians. In fact, the dynamics of the Gaussians can accurately be given by classical mechanics for short times. We label the Gaussians by the ket $|z\rangle$, where

$$(2\hbar\omega)^{-1/2}(\omega\hat{q}+i\hat{p})|z\rangle=z|z\rangle , \tag{2.8a}$$

or

$$\hat{z}|z\rangle=z|z\rangle . \tag{2.8b}$$

The parameter ω is a scale factor that determines the relative uncertainties in p and q; for ω real we have $(\Delta p)^2(\Delta q)^2=\hbar^2/4$. The following relations are also useful:

$$\hat{q}=(\hbar/2\omega)^{1/2}(\hat{z}^\dagger+\hat{z}) , \tag{2.9a}$$

$$\hat{p}=i(\hbar\omega/2)^{1/2}(\hat{z}^\dagger-\hat{z}) , \tag{2.9b}$$

$$\langle z \mid \hat{q} \mid z \rangle = (\hbar/2\omega)^{1/2}\,\mathrm{Re}(z)\ , \tag{2.9c}$$

$$\langle z \mid \hat{p} \mid z \rangle = (\hbar\omega/2)^{1/2}\,\mathrm{Im}(z)\ , \tag{2.9d}$$

$$1 = \int (d^2z/\pi)\mid z\rangle\langle z \mid\ , \tag{2.9e}$$

and

$$\mathrm{Tr}(\hat{A}) = \int (d^2z/\pi)\langle z \mid \hat{A} \mid z\rangle\ , \tag{2.9f}$$

where $d^2z = d(\mathrm{Im}z)d(\mathrm{Re}z)$ in one degree of freedom. In the case of N degrees of freedom, we use nearly the same notation whenever no confusion arises. The relations above allow us to evaluate $Y_{jj}(\mathbf{k},t)$ as

$$Y_{jj}(\mathbf{k},t) = \langle e^{-i\mathbf{k}\cdot\hat{\mathbf{q}}_j} e^{i\hat{H}t/\hbar} e^{i\mathbf{k}\cdot\hat{\mathbf{q}}_j} e^{-i\hat{H}t/\hbar}\rangle \tag{2.10a}$$

$$= \frac{1}{Q}\mathrm{Tr}(e^{-\beta\hat{H}} e^{-i\mathbf{k}\cdot qbhatt_j} e^{i\hat{H}t/\hbar} e^{i\mathbf{k}\cdot\hat{\mathbf{q}}_j} e^{-\hat{H}t/\hbar}) \tag{2.10b}$$

$$= \frac{1}{Q}\int \frac{d^{2N}}{\pi^N}\langle z \mid e^{-\beta\hat{H}} e^{-i\mathbf{k}\cdot\hat{\mathbf{q}}_j} e^{i\hat{H}t/\hbar} e^{i\mathbf{k}\cdot\hat{\mathbf{q}}_j} e^{-i\hat{H}t/\hbar} \mid z\rangle \tag{2.10c}$$

$$= \frac{1}{Q}\int \frac{d^{2N}}{\pi^N}\langle z \mid e^{-\beta\hat{H}/2} e^{-i\mathbf{k}\cdot\hat{\mathbf{q}}_j} e^{i\hat{H}t/\hbar} e^{i\mathbf{k}\cdot\hat{\mathbf{q}}_j} e^{-i\hat{H}t/\hbar} e^{-\beta\hat{H}/2} \mid z\rangle\ , \tag{2.10d}$$

where the $\mid z\rangle$ are the harmonic-oscillator coherent states in N degrees of freedom and $Q = \mathrm{Tr}[e^{-\beta\hat{H}}]$. We focus our attention on the matrix element carrying all the essential information for the correlation function and the spectrum, viz.,

$$\langle z \mid e^{-\beta\hat{H}/2} e^{-i\mathbf{k}\cdot\hat{\mathbf{q}}_j} e^{i\hat{H}t/\hbar} e^{i\mathbf{k}\cdot\hat{\mathbf{q}}_j} e^{-i\hat{H}t/\hbar} e^{-\beta\hat{H}/2} \mid z\rangle \equiv \langle z(\beta) \mid e^{-i\mathbf{k}\cdot\hat{\mathbf{q}}_j} e^{i\hat{H}t/\hbar} e^{i\mathbf{k}\cdot\hat{\mathbf{q}}_j} e^{-i\hat{H}t/\hbar} \mid z(\beta)\rangle\ . \tag{2.11}$$

The state $\mid z(\beta)\rangle \equiv e^{-\beta\hat{H}/2}\mid z\rangle$ is a wave packet, which has been propagated in pure imaginary time an amount $-i\hbar\beta/2$. We can simplify the discussion by approximating the effect of the "temperature propagation." For a given state $\mid z\rangle$, temperature propagation to lowest order (in a cumulant expansion, for example) just weights the state $\mid z\rangle$ by $e^{-\beta H(z)/2}$, where $H(z) = \langle Z \mid \hat{H} \mid z\rangle$. Except for a small correction, which in the case of the coherent state of the harmonic oscillator is just the zero-point energy, $H(z)$ is the classical energy plus the zero-point energy associated with the phase-space point (p,q). For the present qualitative discussion, we take the term $\langle z(\beta) \mid \cdots \mid z(\beta)\rangle$ to be equal to $e^{-\beta H_{\mathrm{cl}}}\langle z \mid \cdots \mid z\rangle$, where H_{cl} is the classical energy of the state $\mid z\rangle$, i.e., $H(p,q)$. (This approximation is made here for purposes of discussion only; in subsequent sections the temperature propagation is analytically or numerically implemented.) We have then

$$Y_{jj}(\mathbf{k},t) \cong \frac{1}{Q}\int \left[\frac{d^{2N}z}{\pi^N}\right]\Phi(z) \times \langle z \mid e^{i\mathbf{k}\cdot\hat{\mathbf{q}}_j} e^{i\hat{H}t/\hbar} e^{i\mathbf{k}\cdot\hat{\mathbf{q}}_j} e^{-i\hat{H}t/\hbar} \mid z\rangle\ , \tag{2.12}$$

where $\Phi(z) = e^{-\beta H_{\mathrm{cl}}(z)}$. It is possible to find a $\Phi(z)$ to replace $e^{-\beta H_{\mathrm{cl}}(z)}$ which makes Eq. (2.12) exact. (See Sec. IV B.) In the high-temperature limit, $\Phi(z)$ indeed becomes $e^{-\beta H_{\mathrm{cl}}(z)}$.

The matrix element in Eq. (2.12) can be evaluated in the Schrödinger picture by allowing the propagators to act upon the states. The state $\mid z\rangle$ is propagated under the Hamiltonian $\hat{H}$ for a time t (propagation), and then the jth particle is promoted to a higher momentum by multiplication by $e^{i\mathbf{k}\cdot\hat{\mathbf{q}}_j}$ (boost) (the expectation value of the momentum of the jth particle is easily shown to be raised by $\mathbf{k}$). The third step involves *backward* propagation for a time t. Finally, the jth particle has its momentum decreased by multiplication by $e^{-i\mathbf{k}\cdot\hat{\mathbf{q}}_j}$. Figure 1(a) shows a phase-space picture of these processes. The essence of this picture is to associate a classical position and momentum distribution (represented as the oval marked "$\mid z\rangle$") with the phase-space localized Gaussian coherent state $\mid z\rangle$, and to represent the effect of propagation $\hat{P} = e^{-i\hat{H}t/\hbar}$, $\hat{P}^\dagger = e^{i\hat{H}t/\hbar}$, boosts, $\hat{B} = e^{i\mathbf{k}\cdot\hat{\mathbf{q}}_j}$, $\hat{B}^\dagger = e^{-i\mathbf{k}\cdot\hat{\mathbf{q}}_j}$, etc. by appropriate displacements and shears in the distributions. The final overlap taken between the two packets in the shaded region. The shading means "take the overlap."

It is quite evident that this way of evaluating the matrix element

$$\langle z \mid e^{-i\mathbf{k}\cdot\hat{\mathbf{q}}_j} e^{i\hat{H}t/\hbar} e^{i\mathbf{k}\cdot\hat{\mathbf{q}}_j} e^{-i\hat{H}t/\hbar} \mid z\rangle = \langle z \mid \hat{B}^\dagger \hat{P}^\dagger \hat{B}\hat{P} \mid z\rangle \tag{2.13}$$

has a rather classical flavor. The two key ideas are (1) to launch the semiclassical approximation from the Schrödinger rather than the Heisenberg picture, and (2) to evaluate the trace in a Gaussian coherent-state basis, making semiclassical evaluation of the matrix elements convenient and physically motivated.

There is another, slightly different phase-space interpretation which serves to illustrate the noncommutativity of $e^{\pm i\hat{H}t/\hbar}$ and $e^{\pm i\mathbf{k}\cdot\hat{\mathbf{q}}_j}$. In Fig. 1(b) we see the effects of allowing the operators $\hat{B}^\dagger$ and $\hat{P}^\dagger$ to act to the left; $\hat{P}$ and $\hat{B}$ act to the right, as before. The propagator P acts first, and then the boost $\hat{B}$ on $\mid z\rangle$, but the order of the propagation and the boost is reversed on the state $\langle z \mid$. The matrix element is finally the overlap between $\hat{B}\hat{P}\mid z\rangle$ and $\hat{P}\hat{B}\mid z\rangle$, the only difference being the order of propagation and boost. Even classically, the changing the order of the operations "propagate" and the "boost" leads to inequivalent final states as seen in Fig. 1(b). The semiclassi-

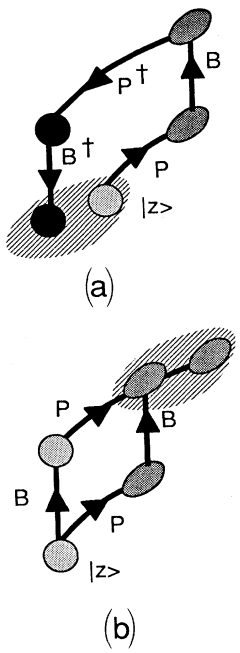

FIG. 1. Phase-space diagrams representing the noncommuting operations governing inelastic neutron scattering. Momentum is the vertical coordinate, position the horizontal. (a) Starting with the state $|z\rangle$, which is a localized wave packet, the matrix element in Eq. (2.13) permits the interpretation shown here, with all four operators acting to the right. The matrix element involves the overlap between the right vector after the four operations and the initial left vector $\langle z|$, as indicated by the shading. In (b) the operators P and B act to the right, and $B^\dagger$ and $P^\dagger$ act to the left. The order of propagation and boost is switched in the two cases, right and left, with the result that the initial wave packet reaches two different locales in phase space. The overlap shown in (a) is the same as in (b).

cal propagation of Gaussian wave packets, outlined in Sec. III, preserves this inequivalence.

The primitive classical approximation to $Y_{jj}(\mathbf{k},t)$, where quantum Heisenberg operators are merely replaced by their classical counterparts, reads

$$Y_{jj}(\mathbf{k},t)=\langle e^{-i\mathbf{k}\cdot\hat{\mathbf{q}}_j}e^{i\mathbf{k}\cdot\hat{\mathbf{q}}_j(t)}\rangle \tag{2.14a}$$

$$=\langle e^{-i\mathbf{k}\cdot[\mathbf{q}_j-\mathbf{q}_j(t)]}\rangle\ , \tag{2.14b}$$

where $\mathbf{q}_j$ and $\mathbf{q}_j(t)$ are purely classical positions. The commutation relations are dropped. Lovesey[5] suggests starting with the exact form

$$Y_{jj}(\mathbf{k},t)=\langle e^{ik\cdot[\hat{\mathbf{q}}_j-\hat{\mathbf{q}}_j(t)]+i\hbar\gamma_{jj}(t)}\rangle\ , \tag{2.14c}$$

where the term $\gamma_{jj}(t)$

$$i\hbar\gamma_{jj}(t)=\tfrac{1}{2}[\mathbf{k}\cdot\hat{\mathbf{q}}_j,\mathbf{k}\cdot\hat{\mathbf{q}}_j(t)]$$
$$+\frac{i}{12}[[\mathbf{k}\cdot\hat{\mathbf{q}}_j,\mathbf{k}\cdot\hat{\mathbf{q}}_j(t)],\mathbf{k}\cdot\hat{\mathbf{q}}_j]$$
$$+\frac{i}{12}[[\mathbf{k}\cdot\hat{\mathbf{q}}_j,\mathbf{k}\cdot\hat{\mathbf{q}}_j(t)],\mathbf{k}\cdot\hat{\mathbf{q}}_j(t)]+\cdots \tag{2.15}$$

contains all the commutation information. Then, $\hat{\mathbf{q}}_j-\hat{\mathbf{q}}_j(t)$ is replaced by its classical counterpart $\mathbf{q}_j-\mathbf{q}_j(t)$, and the commutators are replaced by their classical c-number Poisson bracket analogs ($[\,,\,]\rightarrow i\hbar\{\,,\,\}$). In the case of free motion, the first term in Eq. (2.15) is the only nonvanishing one, and since $\mathbf{q}_j(t)=\mathbf{q}_j+\mathbf{p}_j t$, the classical and quantum brackets give the same result. The improved classical approximation, with $\gamma_{jj}(t)$ included, produces corrections which are simple to use and also give the results exact for the case of a harmonic system. In the case of a general potential, however, an infinite number of terms contribute, and they become increasingly difficult to evaluate, both as the order is increased and as time is increased. Moreover, the higher-order terms become more important as time increases, making this method impractical.

III. SEMICLASSICAL WAVE-PACKET DYNAMICS

The intuitive picture of wave-packet dynamics in the Schrödinger picture has to be augmented by a simple method for the propagation of the packets. A commonly used method is reviewed here.[3(a)–3(f),4,9,10]

The basic idea is illustrated in Fig. 2. A Gaussian packet is launched with specified position q_0 and momentum p_0 on an arbitrary potential. An initially Gaussian packet remains forever Gaussian if the potential is at most quadratic in q, even if the potential is time dependent. The potential shown is anharmonic. Suppose that we replace the true potential by an effective time-dependent quadratic potential which is optimized in some way for the packet being propagated. We choose this optimization by always taking the effective potential to be the locally quadratic Taylor expansion of the true potential *about the instantaneous center of the moving Gaussian.* The idea in this approximation is that the potential is best fit where the wave packet is largest. This approach is simplistic but very easy to implement. It leads to the result Eqs. (3.5c) and (3.5d) that a single classical trajectory calculation, along with its stability equations, suffices to propagate the Gaussian. The price paid for the simplicity is that the "wings" of the Gaussian may be poorly described, since the propagation is optimized for the center. A better semiclassical propagation would involve double-ended boundary conditions and the associated "root searches."[11] Nonetheless, the simpler approach is a true semiclassical method, since the results do become exact as $\hbar\rightarrow 0$. In N dimensions, the most general Gaussian takes the form

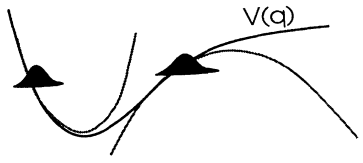

FIG. 2. A potential $V(q)$ is approximated by a quadratic fit in the vicinity of the current position of the wave packet.

$$\langle \mathbf{q} \mid z_t \rangle = \exp\{ i/\hbar [(\mathbf{q}-\mathbf{q}_t)\cdot \mathbf{A}_t \cdot (\mathbf{q}-\mathbf{q}_t) + \mathbf{p}_t \cdot (\mathbf{q}-\mathbf{q}_t) + s_t] \} \ . \tag{3.1}$$

The $N \times N$ matrix $\mathbf{A}_t$, and the N-dimensional vectors $\mathbf{q}_t$ and $\mathbf{p}_t$, and the phase-normalization factor s_t are all specified at $t=0$. Clearly, $\mathbf{q}_t$ and $\mathbf{p}_t$ are $\langle z \mid \hat{\mathbf{q}} \mid z \rangle$ and $\langle z \mid \hat{\mathbf{p}} \mid z \rangle$, respectively. The matrix $\mathbf{A}_t$ describes the "spread" of the wave packet, and its initial value is somewhat arbitrary. However, it should be chosen reasonably, so as to balance the relative uncertainty in position and momentum. A good choice often seems to be to choose $\mathbf{A}_t$ to be the same as the ground-state eigenfunction of the harmonic approximation to the potential, expanded about its minimum. Normalization of the Gaussian requires that

$$\mathrm{Im}(s_{t=0}) = \tfrac{1}{4} i\hbar \ln\{ \det[2\,\mathrm{Im}(\mathbf{A}_{t=0})/\pi\hbar] \} \ . \tag{3.2}$$

(Recall the matrix identity $\det(\mathbf{C}) = \exp\{\mathrm{Tr}[\ln(\mathbf{C})]\}$.) Subsequent integration of the equation of motion for s_t (see below) assures that the wave packet is normalized at all times.

The Gaussian may be fed into the time-dependent Schrödinger equation appropriate to the ansatz described above. It helps to write $\mathbf{A}_t$ as

$$\mathbf{A}_t = \tfrac{1}{2} \mathbf{P}_\mathbf{z} \cdot \mathbf{Z}^{-1} \ , \tag{3.3}$$

where, at $t=0$, the $N \times N$ matrix $\mathbf{Z}$ may be chosen to be the unit matrix, so that $\mathbf{P}_{\mathbf{z},t=0} = 2\,\mathbf{A}_{t=0}$. With the potential expanded as

$$V(\mathbf{q}) = V(\mathbf{q}_t) + \nabla \cdot \mathbf{V}(\mathbf{q}_t) \cdot (\mathbf{q}-\mathbf{q}_t) + \tfrac{1}{2} (\mathbf{q}-\mathbf{q}_t) \cdot \mathbf{V}''(\mathbf{q}_t) \cdot (\mathbf{q}-\mathbf{q}_t) \tag{3.4}$$

we find

$$\frac{d\mathbf{p}_t}{dt} = -\nabla \cdot \mathbf{V}(\mathbf{q}_t) \ , \tag{3.5a}$$

$$\frac{d\mathbf{q}_t}{dt} = \mathbf{p}_t \cdot \mathbf{M}^{-1} \ , \tag{3.5b}$$

$$\frac{d\mathbf{P}_\mathbf{z}}{dt} = -\mathbf{V}''(\mathbf{q}_t) \cdot \mathbf{Z} \ , \tag{3.5c}$$

$$\frac{d\mathbf{Z}}{dt} = \mathbf{P}_\mathbf{z} \cdot \mathbf{M}^{-1} \ , \tag{3.5d}$$

$$\frac{ds_t}{dt} = \mathbf{p}_t \cdot \mathbf{M}^{-1} \cdot \mathbf{p}_t - E + i\hbar\,\mathrm{Tr}(\mathbf{M}^{-1} \cdot \mathbf{A}_t) \ , \tag{3.5e}$$

where $\mathbf{M}$ is the mass matrix, which is normally chosen to be a multiple of the unit matrix, and E is the classical energy of the trajectory $H(\mathbf{q}_t, \mathbf{p}_t)$. Some noteworthy facts about these equations are (1) $\mathbf{q}_t, \mathbf{p}_t$ follow Hamilton's equations of motion, (2) $\mathbf{P}_\mathbf{z}$ and $\mathbf{Z}$ also follow Hamilton's equations, but for a time-dependent, purely quadratic potential given by $\frac{1}{2}\mathbf{Z} \cdot \mathbf{V}''(\mathbf{q}_t) \cdot \mathbf{Z}$, and (3) s_t accumulates the classical action

$$s_t = s_{t=0} + \tfrac{1}{2} i\hbar\,\mathrm{Tr}[\ln(\mathbf{Z} \cdot \mathbf{Z}_{t=0}^{-1})] + \int_0^t (\mathbf{p}_t \cdot \mathbf{M}^{-1} \cdot \mathbf{p}_t - E)\,dt \ . \tag{3.6}$$

Sometimes it is advantageous to "freeze" the $\mathbf{A}$ matrix to its initial value, rather than let it change with time. This is especially true for long-time propagation on significantly anharmonic potentials, where the wave packets may spread so much that the locally quadratic approximation breaks down. The method for frozen $\mathbf{A}$ is called the "frozen Gaussian approximation," or FGA. By default, the original method given above, where $\mathbf{A}_t$ changes with time, is called the "thawed Gaussian approximation," or TGA. In the applications to neutron scattering, the Gaussian parameters $\mathbf{q}_{t=0}, \mathbf{p}_{t=0}$ are chosen according to the phase-space integral $\pi^{-N} \int d^{2N} z \langle z \mid \cdots \mid z \rangle = \pi^{-N} \int d^N \mathbf{p}_0 d^N \mathbf{q}_0 \langle z \mid \ldots \mid z \rangle$. The reader is directed to Ref. 3 for more detailed discussions of wave-packet dynamics.

IV. FIRST APPLICATIONS

We now have the machinery to apply the Schrödinger picture semiclassical wave-packet methods to a wide variety of problems in neutron scattering. Here, we examine two cases where recourse to numerical methods to evaluate the classical trajectories is not necessary.

A. Impulse approximation

Let the operators act on $\mid z(\beta) \rangle$ in the order shown in Eq. (2.13), namely, $\hat{P}$ first, etc. Suppose for the moment that the time-dependent potential $\mathbf{V}$ is quadratic, linear, or constant in $\mathbf{q}$. Then, the $\mathbf{A}_t$ matrix is dependent only upon the initial $\mathbf{A}_{t=0}$ and time, and not the classical position and momentum parameters. This is clear from Eqs. (3.5c) and (3.5d), since $\mathbf{V}''(\mathbf{q}_t)$ is independent of $\mathbf{q}_t$ for quadratic, linear, or constant potentials. Note too that whatever changes that take place in $\mathbf{A}_t$ under the action of $\hat{P}$ are left unchanged by the boost provided by $\hat{B}$. In fact, after the boost we have

$$\langle \mathbf{q} \mid z(t) \rangle = \exp\{ i/\hbar [(\mathbf{q}-\mathbf{q}_t)\cdot \mathbf{A}_t \cdot (\mathbf{q}-\mathbf{q}_t) + (\mathbf{p}_t + \hbar\mathbf{k}) \cdot (\mathbf{q}-\mathbf{q}_t) + \hbar\mathbf{k} \cdot \mathbf{q}_t + s_t] \} \ . \tag{4.1}$$

Because of the boost, backwards time propagation by $\hat{P}^\dagger$ will take the wave packet along a different phase-space path. However, the wave packet will regain its precise initial shape, since the time evolution of $\mathbf{A}_t$ under the effect of $\hat{P}^\dagger$ is just reversed from that of $\hat{P}$, independent of the momentum (and subsequent position) changes caused by the intervening boost. Thus, the backward propagation $\hat{P}^\dagger$ undoes any evolution in the $\mathbf{A}$ matrix. It follows that for these special potentials, we may simply ignore the changes in $\mathbf{A}$ and use "frozen" wave packets, which keep $\mathbf{A}$ fixed. In this case the FGA is exact for the amplitude in Eq. (2.13).

The impulse approximation, as its name suggests, is intended for situations where the momentum transfer $\mathbf{k}$ is large. It will become evident that large $\mathbf{k}$ causes the correlation function to decay rapidly. This allows us to rationalize the use of the FGA for general smooth potentials for large $\mathbf{k}$, since whatever changes in $\mathbf{A}_t$, that take place in a short time are approximately undone for any locally quadratic potential.

The action of the four operators $\hat{P}$, $\hat{B}$, $\hat{P}^\dagger$, $\hat{B}^\dagger$ on $|z\rangle$ has a very simple interpretation. For the case of a free particle we have Fig. 3(a). The abscissa is position and the ordinate is momentum.

We start with a state of a given average position and momentum. The effect of the propagator $\hat{P}$ is to translate the state in position by pt/m. The operator $\hat{B}$ boosts it in momentum by $\hbar k$. Backwards propagation ($\hat{P}^\dagger$) translates it to the left by $(p+\hbar k)t/m$. Finally, $\hat{B}^\dagger$ drops it back down to its original momentum, where it finds itself displaced over by $\hbar kt/m$ relative to the starting state $|z\rangle$. One might imagine that the presence of a potential v would change the relative location of the starting and final states. However, as Fig. 3(b) shows, the distance and displacement in phase space remains the same even with a potential, at least for short times. During the short-time decay of the overlap, the classical mechanics guiding the Gaussians is approximated by

$$p_t = p_0 - \nabla V(q_0)t \ , \tag{4.2a}$$

$$q_t = q_0 + \frac{p_0 t}{m} \ . \tag{4.2b}$$

The displacements that arise for longer times in all but constant potentials can be seen qualitatively from Fig. 1(a).

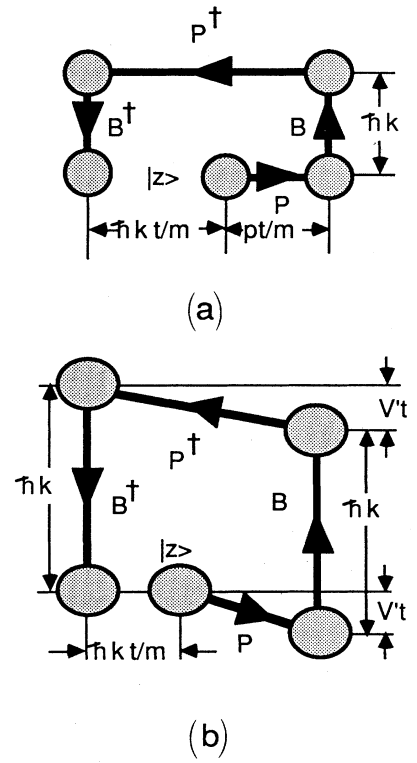

FIG. 3. (a) A wave packet $|z\rangle$ is propagated, boosted, back propagated, and unboosted in a constant potential. The result is a displacement in position. (b) The net short-time effect of the operators P-$B^\dagger$ is seen to be a translation by $\hbar kt/m$, whether or not a potential is present, within the approximation that spreading of the wave packet is neglected (there is no net spreading if the potential is locally quadratic), and with short-time approximations introduced for the classical mechanics.

The distance between the starting and final wave packets is no longer simply $\hbar kt/m$, and the displacement between them now contains a momentum component. The information required to construct this diagram is still purely classical, and it suggests that we may go far beyond the impulse approximation and considerably beyond the usual Heisenberg semiclassical approximations[12] if we are willing to run trajectories and implement the information in the Schrödinger sense. This is one of the main points of this paper.

We are now in a position to calculate

$$Y_{jj}(\mathbf{k},t) = \frac{1}{Q}\int \left[\frac{d^{2N}z}{\pi^N}\right]\Phi(z) \times \langle z \mid e^{-i\mathbf{k}\cdot\hat{\mathbf{q}}} e^{i\hat{H}t/\hbar} e^{i\mathbf{k}\cdot\hat{\mathbf{q}}} e^{-i\hat{H}t/\hbar} \mid z\rangle \ . \tag{4.3}$$

(We are using the diagonal representation of the temperature propagator discussed in Sec. IV B.) As discussed above, the effect of the four operators is to displace $|z\rangle$ by $\hbar k/m$ position. The operator which translates the arguments of functions by q_0 is $e^{iq_0 p/\hbar}$. Thus, except for phase, which is easily shown to be $i\hbar k^2 t/2m$, the operator $e^{i\mathbf{k}\cdot\hat{\mathbf{q}}} e^{i\hat{H}t/\hbar} e^{i\mathbf{k}\cdot\hat{\mathbf{q}}} e^{-i\hat{H}t/\hbar}$ is replaced by $e^{iq_0 p/\hbar}$. We arrive at

$$\langle e^{iq_0 p/\hbar}\rangle e^{i\hbar k^2 t/2m} \ . \tag{4.4}$$

This agrees with Eq. (3.93) in Lovesey.[5] Here, the formula is derived under the assumption of frozen Gaussian wave-packet dynamics for the evolution of $\hat{B}^\dagger \hat{P}^\dagger \hat{B}\hat{P}\,|z\rangle$ with Gaussians guided by classical trajectories. The classical trajectories have been approximated by their short-time expansions.

Lovesey shows that the Fourier transform of $Y_{jj}(\mathbf{k},t)$ is directly related to the momentum distribution of the particles scattering neutron in the sample.

B. Harmonic crystal

Our strategy will be to implement Eq. (2.12) in a way that suggests the procedure for anharmonic cases. We do, however, use the diagonal representation of the thermal-density operator with the exact $\Phi(z)$, which is known in the case of a harmonic oscillator. For a one-dimensional harmonic oscillator, $\Phi(z)$ can be shown to be[13]

$$\Phi(z) = 2\pi\hbar \exp\left[-\frac{1}{2\hbar\omega}(e^{\beta h\omega}-1)(p^2/m + m\omega^2 q^2)\right] , \tag{4.5a}$$

$$\Phi(z) = 2\pi\hbar \exp\left[-\frac{1}{\hbar\omega}(e^{\beta h\omega}-1)H_{\rm cl}(p,q)\right] , \tag{4.5b}$$

where

$$H_{\rm cl}(p,q) = \frac{1}{2m}p^2 + \tfrac{1}{2}m\omega^2 q^2 \ .$$

Note that $H_{\rm cl}(p,q)$ is the classical Hamiltonian. In the limit of large temperature, $(1/2\hbar\omega)(e^{\beta\hbar\omega}-1)\to\beta/2$, thus $\Phi(z)\to e^{-\beta H_{\rm cl}}$ as expected, and, as $T\to 0$, $\Phi(z)\to\delta(p)\delta(q)$, also as expected. In this case, Eq. (2.12) reduces to the evaluation of a single state $|z\rangle$, namely, the ground harmonic-oscillator state.

The expression that we need to evaluate is then

$$Y_{jj}(\mathbf{k},t)=\frac{1}{Q}\int\left[\frac{d^2z}{\pi}\right]\Phi(z)\langle z\mid e^{-i\mathbf{k}\cdot\hat{\mathbf{q}}_j}e^{i\hat{H}t/\hbar}e^{i\mathbf{k}\cdot\hat{\mathbf{q}}_j}e^{-i\hat{H}t/\hbar}\mid z\rangle \tag{4.6a}$$

$$=\frac{1}{Q}\int\left[\frac{d^2z}{\pi}\right]\Phi(z)\langle z\mid e^{-i\hat{H}t/\hbar}e^{-i\mathbf{k}\cdot\hat{\mathbf{q}}_j}e^{i\hat{H}t/\hbar}e^{i\mathbf{k}\cdot\hat{\mathbf{q}}_j}\mid z\rangle\ . \tag{4.6b}$$

There are many elegant shortcuts to the essential harmonic crystal results starting with Eq. (4.6) involving operator algebra identities, etc. However, these shortcuts merely lead back to the traditional derivation of neutron scattering for the harmonic oscillator and remove emphasis from the way a calculation involving more complicated potentials would proceed. Section V presents results for an anharmonic, nonseparable potential model for HCN in a crystal, and the present derivation of the harmonic oscillator serves as an introduction for the methods used there.

A word about the role of $\Phi(z)$ is in order. First, Eqs. (2.10), the governing equations, make no use of $\Phi(z)$ and require imaginary time propagation. Such propagation is not particularly dangerous or difficult, except at low temperatures. At absolute zero, the situation is again simple, since the system is at rest and describable by a single (many-body) wave packet. In the case of harmonic systems, we have shown that a $\Phi(z)$ may be found which gives exact results [Eq. (4.5)]. For anharmonic systems at finite temperature, either we have to do an imaginary time propagation or we need to find a modified $\Phi(z)$ which accounts for the anharmonicity. There is as yet little experience with either of these alternatives.

The matrix element appearing in Eq. (4.6) can be viewed as the overlap between $e^{-i\hat{H}t/\hbar}\mid z\rangle$ and $e^{-i\mathbf{k}\cdot\hat{\mathbf{q}}_j}e^{-i\hat{H}t/\hbar}e^{i\mathbf{k}\cdot\hat{\mathbf{q}}_j}\mid z\rangle$. (We specialize to a one-dimensional harmonic oscillator for notational simplicity.) In coordinate space, $\mid z\rangle$ reads

$$\langle q\mid z_0\rangle=\exp\left[\frac{i}{\hbar}\left[\frac{im\omega}{2}(q-q_0)^2+p_0(q-q_0)+\gamma_0\right]\right]\ . \tag{4.7}$$

We have added a subscript 0 to $\mid z\rangle$ and its parameters to indicate the initial, unpropagated, and unboosted $\mid z\rangle$. After propagation, $\mid z_0\rangle$ becomes $\mid z_1\rangle$,

$$\langle q\mid e^{-i\hat{H}t/\hbar}\mid z_0\rangle=\langle q\mid z_1\rangle=\exp\left[\frac{i}{\hbar}\left[\frac{im\omega}{2}(q-q_1)^2+p_1(q-q_1)+\gamma_1\right]\right] \tag{4.8}$$

where

$$q_1=q_0\cos(\omega t)+\frac{p_0}{m\omega}\sin(\omega t)\ , \tag{4.9a}$$

$$p_1=p_0\cos(\omega t)-m\omega q_0\sin(\omega t)\ , \tag{4.9b}$$

$$\gamma_1=\gamma_0+\sin(2\omega t)\frac{p_0^2/m-q_0^2m\omega^2}{4\omega}+q_0p_0\frac{\cos(2\omega t)-1}{2}\ . \tag{4.9c}$$

For the evaluation of $\mid z_2\rangle=e^{-i\mathbf{k}\cdot\hat{\mathbf{q}}}e^{-i\hat{H}t/\hbar}e^{i\mathbf{k}\cdot\hat{\mathbf{q}}}\mid z_0\rangle$ first note that the effect of the boost is just to raise p_0 to $p_0+\hbar k$,

$$e^{i\mathbf{k}\cdot\hat{\mathbf{q}}}\mid z_0\rangle=\exp\left[\frac{i}{\hbar}\left[\frac{im\omega}{2}(q-q_0)^2+(p_0+\hbar k)(q-q_0)+\hbar kq_0+\gamma_0\right]\right]\ . \tag{4.10}$$

We may again use Eqs. (4.9), with p_0 replaced by $p_0+\hbar k$, and finally reduce the momentum by $-\hbar k$, corresponding to $e^{-i\mathbf{k}\cdot\hat{\mathbf{q}}}$,

$$q_2=q_0\cos(\omega t)+\frac{(p_0+\hbar k)}{m\omega}\sin(\omega t)\ , \tag{4.11a}$$

$$p_2=(p_0+\hbar k)\cos(\omega t)-m\omega q_0\sin(\omega t)-\hbar k\ , \tag{4.11b}$$

$$\gamma_2=\gamma_0+\frac{1}{4\omega}\sin(2\omega t)[(p_0+\hbar k)^2/m-q_0^2m\omega^2]+\tfrac{1}{2}q_0(p_0+\hbar k)[\cos(2\omega t)-1]-k(q_2-q_0)\ . \tag{4.11c}$$

Now, the overlap between $\mid z_1\rangle$ and $\mid z_2\rangle$ is

$$\langle z_1\mid z_2\rangle=\exp\left[-\frac{m\omega}{4\hbar}(q_2-q_1)^2-\frac{1}{4m\omega\hbar}(p_2-p_1)^2-\frac{i}{2\hbar}(q_2-q_1)(p_2+p_1)+\frac{i}{\hbar}(\gamma_2-\gamma_1^*)\right]\ . \tag{4.12}$$

In a calculation involving anharmonic potentials, the $p_1,\ldots,\gamma_1,p_2,\ldots,\gamma_2$ are all determined numerically by solving the classical equations of motion. For the case of frozen Gaussian propagation, the overlap (4.12) still holds, whereas if the Gaussian has been allowed to spread (TGA), a slightly more complicated overlap formula holds.[3c] For the $\mid z_1\rangle$ and $\mid z_2\rangle$ given above, Eq. (4.12) yields

$$\langle z_1\mid z_2\rangle=\langle z_0\mid e^{i\hat{H}t/\hbar}e^{-i\mathbf{k}\cdot\hat{\mathbf{q}}}e^{-i\hat{H}t/\hbar}e^{i\mathbf{k}\cdot\hat{\mathbf{q}}}\mid z_0\rangle$$
$$=\exp\{-[k^2\hbar^2/(2m\omega\hbar)+ikq_0][1-\cos(\omega t)]-ik/(m\omega)(p_0+\hbar k/2)\sin(\omega t)\}\ . \tag{4.13}$$

Equation (4.6) becomes

$$Y(\mathbf{k},t)=\int dp_0 dq_0 \exp\left[-\frac{1}{\hbar\omega}(e^{\beta h\omega}-1)H_{\rm cl}(p_0,q_0)\right]$$
$$\times\exp\left[-\left[\frac{k^2\hbar^2}{2m\omega\hbar}+ikq_0\right][1-\cos(\omega t)]-\frac{ik}{m\omega}(p_0+\hbar k/2)\sin(\omega t)\right]$$
$$=\exp\left[-\left\{\frac{k^2\hbar^2}{2m\omega\hbar}\left[[1-\cos(\omega t)]\coth\left[\frac{\beta\hbar\omega}{2}\right]-i\sin(\omega t)\right]\right\}\right] . \quad (4.14)$$

The last line of Eq. (4.14) agrees with Lovesey, Eqs. (3.143) and (3.144), as indeed it must. We have derived it here with the aid of the exact dynamics of coherent-state wave packets.

C. Replacement by a single wave packet

Note the similarity between the overlap $\langle z_1 | z_2\rangle$, Eq. (4.13), which represents the fate of a single wave packet, and the finite temperature correlation function $Y(\mathbf{k},t)$, Eq. (4.14). In fact, if we take $q_\beta=0$, and

$$p_\beta=\hbar k/2[1/\lambda-\lambda] ,$$

where

$$\lambda=[\coth(\beta\hbar\omega/2)]^{1/2} ,$$

then

$$Y(\mathbf{k},t)=\langle z_\beta | e^{i\hat{H}t/\hbar}e^{-i\mathbf{k}\cdot\hat{\mathbf{q}}}e^{-i\hat{H}t/\hbar}e^{i\mathbf{k}\cdot\hat{\mathbf{q}}} | z_\beta\rangle , \quad (4.15)$$

where $|z_\beta\rangle$ is the wave packet defined by q_β and p_β. This is a rather peculiar result, which allows the infinite sum over all initial states required in Eq. (4.6), to be replaced by a single state $|z_\beta\rangle$. This result carries directly over to any number of normal modes i, simply as

$$Y_{jj}(\mathbf{k},t)=\langle z_\beta | e^{-i\mathbf{k}\cdot\hat{\mathbf{q}}_j}e^{i\hat{H}t/\hbar}e^{i\mathbf{k}\cdot\hat{\mathbf{q}}_j}e^{-i\hat{H}t/\hbar} | z_\beta\rangle , \quad (4.16)$$

where $q_{i\beta}=0$

$$p_{i\beta}=\hbar k_i/2[1/\lambda_i-\lambda_i] ,$$

and

$$\lambda_i=[\coth(\beta\hbar\omega_i/2)]^{1/2} ,$$

where ξ_i is the ith normal mode coordinate and

$$\sum_i k_{ji}\xi_i \mathbf{k}\cdot\mathbf{q}_j .$$

The harmonic multimode case splits up into a separable product of single-mode correlation functions, i.e.,

$$Y_{jj}(\mathbf{k},t)=\prod_i \langle z_{i\beta} | e^{-ik_{ji}\xi_i}e^{i\hat{H}_i t/\hbar}e^{ik_{ji}\xi_i}e^{-i\hat{H}_i t/h} | z_{i\beta}\rangle \quad (4.16b)$$
$$=\prod_i \exp\left\{-\frac{k_{ji}^2\hbar^2}{2m\hbar\omega_i}\left[[1-\cos(\omega_i t)]\coth\left[\frac{\beta\hbar\omega_i}{2}\right]-i\sin(\omega_i t)\right]\right\} \quad (4.16c)$$
$$=\exp\left\{-\sum_i\frac{k_{ji}^2\hbar^2}{(2m\hbar\omega_i)}\left[[1-\cos(\omega_i t)]\coth(\beta\hbar\omega_i/2)-i\sin(\omega_i t)\right]\right\} \quad (4.16d)$$
$$\equiv\exp[-2W(\mathbf{k},t)] . \quad (4.16e)$$

D. Separation of time scales and the Debye-Waller Factor

Recently, Griffin and Jobic[14(a)] have made an interesting point regarding the appearance of one-, two-, ···, phonon structure in the inelastic incoherent neutron scattering under conditions of large energy transfer and very small Debye-Waller factor. According to these authors, it had been assumed that the small Debye-Waller factor would extinguish the possibility of vibrational structure in the cross section. This is not the case under certain circumstances, and the Griffin and Jobic paper explains why, in terms of the "time-dependent Debye-Waller factor" and a separation of timescales between the high- and low-frequency modes. The time-dependent Debye-Waller factor is just $\exp[-2W(\mathbf{k},t)]$ of Eq. (4.16e). The structure in the cross section, in spite of large energy transfer, occurs if $\exp[-2W(\mathbf{k},t)]$ oscillates at a vibrational frequency characteristic of a high-frequency local mode, during its decay toward a nearly vanishing asymptote at long times. The cross section has to reflect these oscillations with corresponding frequency oscillations of its own, spaced by the frequency of the local mode and broadened by the overall long-time decay.

The high-frequency modes are simply local lattice vibrations which are excited by the neutron scattering event, and which also decay since they are not normal modes. However, most of the long-time decay of the time-

dependent Debye-Waller factor is due to the effect of the low-frequency modes, whose net momentum displacement is large, but whose decay is slow simply because the modes are of low frequency.

The persistence of vibrational structure in the presence of large energy transfer is analogous to the "pseudolocalized-phonon" structure in the phonon sidebands of electronic transition in mixed molecular crystals.[15]

In the case of a harmonic lattice, Griffin and Jobic[14(a),14(b)] [see also Ref. 14(c)] recommend the direct evaluation of the time-dependent Debye-Waller factor $\exp[-2W(\mathbf{k},t)]$, followed by Fourier transform into the frequency domain to get the cross section. One advantage of this approach is that the experimental cross-section data is always obtained with some finite resolution whether because of the intrinsic continuum of modes (save for the zero-phonon peak), or because of instrumental resolution. Given this situation, the time-dependent Debye-Waller factor $\exp[-2W(\mathbf{k},t)]$ only needs to be calculated for a finite time corresponding to the experimental resolution.

We wish to emphasize that our wave packet approach shares the same advantages, with the important addition that our methods are directly applicable to the anharmonic case.

We have derived Eq. (4.16e) using wave packet techniques which, it should be recalled, are exact for any harmonic potential. Thus Eq. (4.16e) is the exact expression for the harmonic case and it agrees with the Griffin and Jobic analysis.

E. The Wigner representation

Some additional insight into the semiclassical nature of neutron scattering may be had by study of the Wigner phase-space formulation of quantum mechanics. The following discussion is not self-contained as it assumes some knowledge of the Wigner formulation. Excellent references on the Wigner phase-space method (a formulation entirely equivalent to quantum mechanics) are readily available,[16] including the seemingly neglected Rosenbaum and Zweifel paper.[16(a)] We present only the "bottom line" formula for $Y_{jj}(\mathbf{k},t)$.

One of us has previously discussed the potential and the pitfalls of semiclassical approaches based on the Wigner phase-space theory.[17] We translate the Rosenbaum and Zweifel results for the case of neutron scattering from a harmonic system into the current notation, for the case of one dimension,

$$Y(k,t)=\int dp_0 dq_0 \rho_w(p_0,q_0) e^{-ikq_0} e^{k/2\nabla_p} e^{ikq_t} , \tag{4.17}$$

where $q_t = q_0\cos(\omega t)+(p_0/m\omega)\sin(\omega t)$, $\nabla_p = \partial/\partial p_0$ and

$$\rho_w(p_0,q_0)=\frac{1}{\pi h}\tanh(\beta h\omega/2) \times \exp\left[-\frac{2}{h\omega}\tanh(\beta h\omega/2)H_{\rm cl}(p_0,q_0)\right]$$

is the Wigner phase-space density for an oscillator. It is interesting to note that since

$$e^{k/2\nabla_p} f(p)=f(p+\tfrac{1}{2}k) ,$$

Eq. (4.17) can be written

$$Y(k,t)=\int dp_0 dq_0 \rho_w(p_0,q_0) \times e^{-ikq_0} e^{ikq_t(q_0,p_0+\hbar k/2)} , \tag{4.18}$$

where

$$q_t(q_0,p_0+\hbar k/2) = q_0\cos(\omega t)+(p_0+\hbar k/2)/(m\omega)\sin(\omega t) . \tag{4.19}$$

Carrying out the integrations gives exactly the same results as before for $Y(k,t)$. Note that $\rho_w(p_0,q_0)$ and $\Phi(z)=2\pi\hbar\exp[-(1/\hbar\omega)(e^{\beta\hbar\omega}-1)H_{\rm cl}(p,q)]$ are somewhat different. Both become proportional to $e^{-\beta H_{\rm cl}(p_0,q_0)}$ as $T\to\infty$.

The time evolution of $q_t(q_0,p_0+\hbar k/2)$ is entirely classical. It is intriguing that Eq. (4.18) implies that the exact correlation function may be had by (1) using the Wigner phase-space distribution appropriate to the undisturbed equilibrium state of the oscillator as a sampling density, and (2) computing the classical correlation function $e^{-ikq_0}e^{ikq_t(q_0,p_0+\hbar k/2)}$ over this density.[7] Note that the correlation function is for the oscillator boosted by half the momentum transfer $\hbar k$.

V. APPLICATION TO HCN

We do not attempt a complete treatment of incoherent inelastic neutron scattering from crystalline HCN, but rather consider only the anharmonic intramolecular modes (two stretches, two bends). If one is willing to considerably escalate the effort of setting up the calculation and the computation time, it is now technically possible to examine a fully coupled lattice of HCN molecules at the level of Gaussian wave-packet dynamics.

The incoherent cross section for hydrogen is much larger than that of the C or N atoms, and we accordingly assume in our calculations that all of the momentum transferred is given to the hydrogen. This momentum transfer has effects on the rotation and center-of-mass translation of the molecule (which in the crystal are really librational and center-of-mass vibrational motions), but the contributions of these degrees of freedom are ignored. The momentum transfer to the two stretches and two bends are computed and the subsequent wave-packet dynamics is calculated in the potential energy surface described below. This surface is fairly sophisticated by present standards, including anharmonicities, coupling between modes, etc. Our calculations are for 0 K, and so the integrals over initial wave-packet states in Eq. (2.10) reduce to the ground state $|0\rangle$, i.e.,

$$Y_{jj}=\langle 0|e^{-i\mathbf{k}\cdot\hat{\mathbf{q}}_j}e^{i\hat{H}t/\hbar}e^{i\mathbf{k}\cdot\hat{\mathbf{q}}_j}e^{-i\hat{H}t/\hbar}|0\rangle \equiv C(t) . \tag{5.1}$$

We have used the FGA throughout these calculations. Some aspects of the results might be improved by using the TGA. Best (indeed completely accurate for the poten-

tial surface assumed) results could be obtained for significantly increased effort by using time-dependent variational propagation of the wave packets, in which several traveling together in bundles are considered to be a basis set for the time-dependent Schrödinger Equation.[3(b),4(a)–4(c),17]

A. Coordinates and potentials

We use normal coordinates to describe the potential surfaces and dynamics. These coordinates allow an approximate separation of vibrational, rotational (or librational in the crystal) and translational modes, permitting the problem to be described by just four variables. The major disadvantage to the use of normal coordinates is that they usually provide a poor description of the molecular surface, especially at large displacements from equilibrium. Bond lengths and angles provide a much better description of the potential energy surface; but the kinetic energy is very complicated in these coordinates. Here a set of variables is described that does provide a good description of the potential surface while being simple functions of the normal coordinates. A potential surface for gas-phase HCN is constructed, and it is modified to accommodate the effects of the presence of neighboring molecules in a crystal. Carter, Mills, and Murrell[18(a)] have determined gas-phase potential surface for HCN, and *ab initio* surfaces are also available. We choose not to use these surfaces but to modify the older spectroscopic potential of Strey and Mills.[18(b)] This potential was obtained by deducing the derivatives of the potential surface, evaluated at the equilibrium geometry, from spectroscopic data. Hoy, Mills, and Strey then performed a nonlinear transformation[18(c)] of the normal coordinates into a set of coordinates that closely resembles the bond lengths and angles; the resulting potential surface has the same derivatives up to fourth order as the corresponding potential surface written in terms of the bond lengths and angles. Following Hoy, Mills, and Strey, we define these variables as

$$S_i = \sum_r L_i^r Q_r + \tfrac{1}{2}\sum_{r,s} L_i^{rs} Q_r Q_s + \tfrac{1}{6}\sum_{r,s,t} L_i^{rst} Q_r Q_s Q_t \ , \tag{5.2}$$

where Q_i are the normal coordinates, determined from the Strey and Mills potential, and the elements of the L tensors are known functions of the equilibrium geometry and normal coordinates.[18] Two of the S coordinates, S_h and S_n, represent the displacement of the CH and CN bond lengths from equilibrium, respectively. Some choice is possible, as to which two geometric variables the remaining bending coordinates are to resemble. If the linear molecule is taken to lie on the y axis, $\delta\theta$ is the displacement of the HCN bond angle from linearity, and α is the angle describing the rotation of the plane of the bent molecule from the x-y plane, then we choose

$$S_x = \sin(\delta\theta)\cos\alpha \tag{5.3a}$$

and

$$S_z = \sin(\delta\theta)\sin\alpha \ . \tag{5.3b}$$

These coordinates display the correct symmetry, i.e., that

$$S_\theta^2 = S_x^2 + S_z^2$$

is independent of α. Strey and Mills[18(b)] determined the derivatives of the potential with respect to the S variables. We do not introduce the approximation that the bond lengths and angles may be substituted for these variables, as do Strey and Mills, but proceed directly. The derivative information available here may be used to construct a power-series expansion potential, but such a potential has incorrect boundary conditions at large bond lengths. Simons, Parr, and Finlan[19] have shown that it is preferable to write the power-series expansion in the variables

$$X_h = S_h/(S_h + r_h^0) \ , \tag{5.4a}$$

$$X_n = S_n/(S_n + r_n^0) \ , \tag{5.4b}$$

where r_h^0 and r_n^0 are equilibrium CH and CN bond lengths, respectively. Use of these variables greatly improves the boundary properties at large stretch displacements, and results in a potential which is much more accurate in these regions. The final potential for gas-phase HCN is written as

$$\begin{aligned} V_g = {} & \tfrac{1}{2}(f_{hh}X_h^2 + f_{hn}X_hX_n + f_{nn}X_n^2 + f_{\theta\theta}S_\theta^2) + \tfrac{1}{6}(f_{hhh}X_h^3 + f_{hhn}X_h^2X_n + f_{hnn}X_hX_n^2 + f_{nnn}X_n^3 + f_{h\theta\theta}X_hS_\theta^2 + f_{n\theta\theta}X_nS_\theta^2) \\ & + \tfrac{1}{24}(f_{hhhh}X_h^4 + f_{hhhn}X_h^3X_n + f_{hhnn}X_h^2X_n^2 + f_{hnnn}X_hX_n^3 + f_{nnnn}X_n^4 \\ & + f_{hh\theta\theta}X_h^2S_\theta^2 + f_{hn\theta\theta}X_hX_nS_\theta^2 + f_{nn\theta\theta}X_n^2S_\theta^2 + f_{\theta\theta\theta\theta}S_\theta^4) \end{aligned} \tag{5.5}$$

and is implicitly a function of the normal coordinates. The force constants contained therein are selected so as to give the same derivatives at the equilibrium geometry as deduced by Strey and Mills from experiment. Their values are given in Table I. This potential is expected to be quite accurate as similar functions have been successful at describing the potential surface of water.[20–23] Note that the harmonic vibration frequencies resulting from this potential are identical to the harmonic frequencies of the original Strey and Mills potential.

In the crystal this gas-phase intermolecular potential is perturbed by the neighboring molecules. If we included all of the degrees of freedom of this problem by modeling the entire crystal lattice then this perturbation would be automatically included. This approach is feasible as intermolecular potential surfaces for HCN are known,[21] but is not pursued here because of its complexity. An empirical method for determining the effect of the presence of neighboring molecules is to assume that only the harmonic-force constants change and that the anharmonic ones

TABLE I. Force constants mdyne Å^n; (mdyne Å$=10^{-18}$J); the equilibrium bond lengths used are $r_h^0=1.06549$ Å, $r_n^0=1.15321$ Å.

Constant	V_g	V_c
f_{hh}	7.0966	6.3448
f_{hn}	−0.4915	−0.4915
f_{nn}	24.8730	25.0654
$f_{\theta\theta}$	0.2596	0.3553
f_{xz}	0.0000	0.0084
f_{hhh}	−0.2048	−0.2048
f_{hhn}	0.1571	−1.3174
f_{hnn}	1.7429	0.2684
f_{nnn}	−43.9248	−43.9248
$f_{n\theta\theta}$	−2.2488	−2.2488
f_{hhhh}	−24.1390	−24.1390
f_{hhhn}	1.4494	−4.6411
f_{hhnn}	12.6822	14.3843
f_{hnnn}	1.4494	−4.6411
f_{hhnn}	12.6822	14.3843
f_{hnnn}	14.8563	8.0452
f_{nnnn}	−396.3783	−396.3783
$f_{nn\theta\theta}$	0.7493	−1.6800
$f_{hn\theta\theta}$	0.0000	0.0000
$f_{nn\theta\theta}$	2.2342	−6.7608
$f_{\theta\theta\theta\theta}$	0.0316	0.0316
f_{xxzz}	0.0000	0.0000

remain the same. This assumption is a key feature in the Rice-Sceats model of water.[22] (See also Ref. 23.) Adopting the spirit of this approach, we adjust only the second-order constants in V_g; the anharmonicities are affected as well because of our use of Simons-Parr-Finlan coordinates. A further complication arises, however, in that the high-temperature HCN crystal lattice is body-centered tetragonal and thus the degeneracy of the bending vibrations is lifted. In order to account for this effect, two new terms are added to the gas-phase potential, and the complete crystal potential is written as

$$V_c = V_g + f_{xz}S_xS_z + f_{xxzz}S_x^2S_z^2 \ . \tag{5.6}$$

Initially we set f_{xxzz} to zero and adjust f_{hh}, f_{nn}, $f_{\theta\theta}$, and f_{xz} to account for the change in the infrared vibration frequencies upon crystal formation. Table I also includes the values of the potential constants used in the crystal potential. The harmonic vibration frequencies of both potentials are given in Table II, along with the observed infrared frequencies.[24] Insufficient experimental information is available to determine a value for f_{xxzz}. This force constant does not affect the separation of the bend fundamentals though it does split levels at higher energy. Its value is used as an adjustable parameter in the following calculations and the calculated inelastic neutron spectra are quite sensitive to it.

The absolute value of the incoherent inelastic cross section, as given by Eq. (2.1), is strongly influenced by the prefactor k'/k and therefore by the experimental scattering conditions. But the momentum transfer $\mathbf{k}$ is the most important quantity, and we restrict ourselves to calculating spectra of relative scattering intensities for given, fixed values of $\mathbf{k}$. In an actual experiment many different momentum transfers $\mathbf{k}$ are involved simultaneously. But for each fixed initial $\mathbf{k}_{\rm in}$ and final $\mathbf{k}_{\rm out}$ the value of $\mathbf{k}=\mathbf{k}_{\rm out}-\mathbf{k}_{\rm in}$ is uniquely defined. Thus, by varying, for example, the initial neutron beam energy and the orientation of the crystal, and by scanning the final scattering angle, the spectrum for one fixed $\mathbf{k}$ can be extracted from a series of measurements. On the other hand, for direct comparison with a given measurement, a series of calculations could be carried out with scattering parameters $\mathbf{k}, \mathbf{k}_{\rm in}$, and $\mathbf{k}_{\rm out}$, chosen according to the kinematics of the experiment.

TABLE II. Harmonic and Observed Frequencies (cm^{-1}).

Mode	Gas		Crystal	
	Observed	Harmonic	Observed	Harmonic
ω_1	3312	3442	3132	3268
ω_2	2089	2129	2097	2128
ω_{2a}	712	727	838	855
ω_{2b}	712	727	828	845

In the present calculations the y axis is chosen along the axis of the linear HCN molecules; x and z directions are perpendicular to this axis.

B. Results

Spectra of relative scattering intensities are plotted in Fig. 4. The results are for incoherent inelastic neutron-HCN scattering and for the modified crystal potential with force constants, as given in Table I. The quartic bend-bend coupling constant f_{xxzz} [see Eq. (5.6)] is set to zero.

For the results in the top panel of Fig. 4, the Fourier time transformation in Eq. (2.2) is taken over 600 constant time steps, with Gaussian time domain damping in-

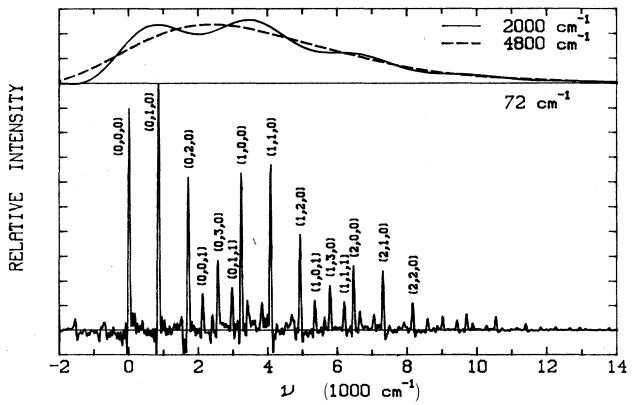

FIG. 4. Neutron inelastic scattering from HCN, for a particular choice of momentum transfer. See text for details.

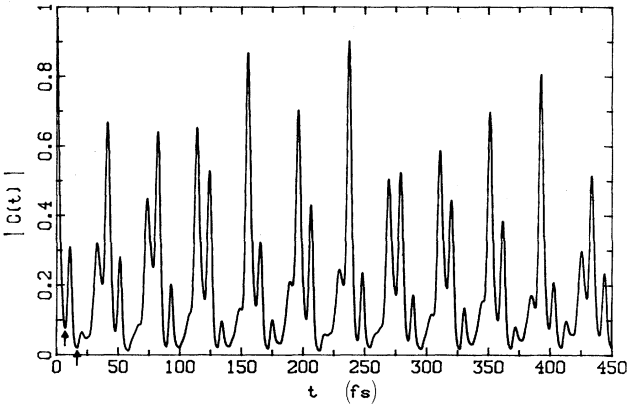

FIG. 5. The absolute value of the autocorrelation function used to generate Fig. 4.

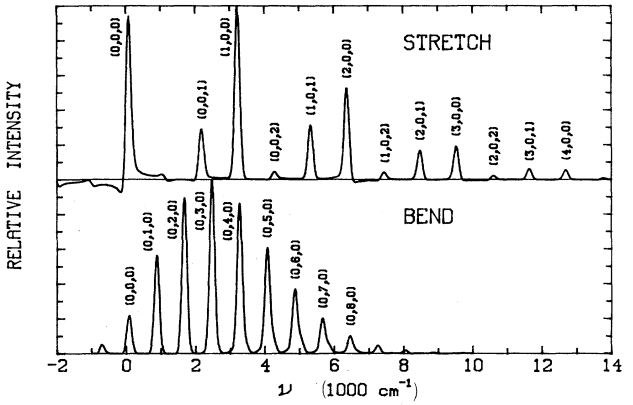

FIG. 6. Two additional choices for momentum transfer, for head-on collision (along the molecular axis for HCN), top, and perpendicular to the axis, bottom.

cluded to given 2000- and 4800-cm^{-1} resolution. The time unit of each step is $1/(20\pi)$ of the period of the fastest vibration, or 0.154 23 fs. Figure 4, lower panel, is for 3000 time steps with a resolution of 72 cm^{-1}.

The momentum transfer in both parts of Fig. 4 is given by $\Delta P_x = 0.0$, $\Delta P_y = 80.$, $\Delta P_z = 60.$ in units of amu Å/ps. In these units a momentum of $|P| = 98.65$ corresponds to a neutron energy of 0.5 eV or 4030 cm^{-1}. A momentum transfer in this direction leads to a simultaneous excitation of the HCN stretch and bend modes, as is revealed in the rich spectral structure. In the low-resolution spectrum of Fig. 4 only the fast ν_1-stretch mode with an energy spacing of ~ 3100 cm^{-1} (see Table II) is clearly resolved. The higher resolution spectrum of Fig. 4 is dominated by a peak spacing of ~ 830 cm^{-1}, associated with the bending motion. The ν_1 stretch now reveals itself as a superposed intensity modulation. In addition, at least the first excited state of the ν_3 stretch is visible as a peak around 2100 cm^{-1}. The small 10-cm^{-1} energy spacing of the two bending modes is not visible with the given resolution.

In general, the initial momentum kick transfers vibrational, translational, and rotational (really librational in a crystal) energy to the molecule. Of the total transferred energy of about 4030 cm^{-1} only the vibrational part is used in our present calculations. The maximum intensities in the generated spectra are then found around the classical energy, contained in molecular vibrations. This energy is 3643 cm^{-1} for Fig. 4 and 3022 cm^{-1} for Figs. 6 and 7.

For the spectrum in Fig. 4, the absolute value of the autocorrelation function $|C(t)|$ [see Eq. (5.1)] is plotted in Fig. 5. Almost 12 periods of the slower bending motion and about 47 ν_1-stretch periods are mirrored in this autocorrelation function. The arrows indicate the longest time data used in constructing the 2000- and 4800-cm^{-1} resolution spectra shown in Fig. 5. The band contour, 4800-cm^{-1} resolution, is obtained from the initial decay of the overlaps, while choosing the first recurrence in the overlap gives the fine structure seen in the 2000-cm^{-1} spectra.

Spectra with two other selective initial momentum kicks are shown in Fig. 6. The top panel is for $\Delta P_x = 0.0$, $\Delta P_y = 100$, $\Delta P_z = 0.0$, i.e., for a head-on collision with initial momentum transfer along the HCN axis only. The direction of ΔP in the bottom panel is perpendicular to the molecular axis: $\Delta P_x = 0.0$, $\Delta P_y = 0.0$, $\Delta P_z = 100$. The units are again amu Å/ps. All potential parameters are the same as for the results in Fig. 4, and the resolution is 72 cm^{-1}, as in Fig. 4, bottom panel. As expected, the head-on collision (Fig. 6, top) leads to excitation of the two stretch modes and their combinations only. An initial kick of the H atom in z direction (Fig. 6, bottom) results in a spectrum with a peak spacing corresponding to the bending frequency. As the bending motion of the molecule is coupled to the stretch, a spectrum with this ΔP at even higher resolution should show the effect of the stretch motion as additional structure as well.

The results in Figs. 4–6 are for a potential that can be expected to give a realistic description of the intramolecular HCN dynamics, at least at lower energies. The spectra in Fig. 7 are obtained with a nonzero value for f_{xxzz} in Eq. (5.6). However, there are no experimental data to obtain a value for f_{xxzz}. We choose for f_{xxzz} a value of 0.047 87 mdyne, corresponding to a coupling in reduced units of 0.175, and leave all of the other potential parameters unchanged. The anharmonic coupling term between the two bends has a qualitative effect on the bending-mode spectra, as shown in Fig. 7. The top panel in Fig. 7 is for a simultaneous and equal momentum transfer in the x and z direction: $\Delta P_x = \Delta P_z = 70.71$, $\Delta P_y = 0.0$ amu Å/ps. In this direction the term $f_{xxzz} S_x^2 S_z^2$ has its largest value. The potential is steeper and the result is a higher frequency. This is seen in the top panel where the peak spacing is clearly large, when compared with the remaining panels. These are for successively more momentum transfer into the x mode at the expense of the z mode. (0° means $\Delta P_x = 100$, $\Delta P_z = 0.$)

In the case of 0-K scattering we can write

$$e^{-i\hat{H}t/\hbar}|0\rangle = e^{-iE_0 t/\hbar}|0\rangle \ , \tag{5.7}$$

where E_0 is the energy of the ground state of the system.

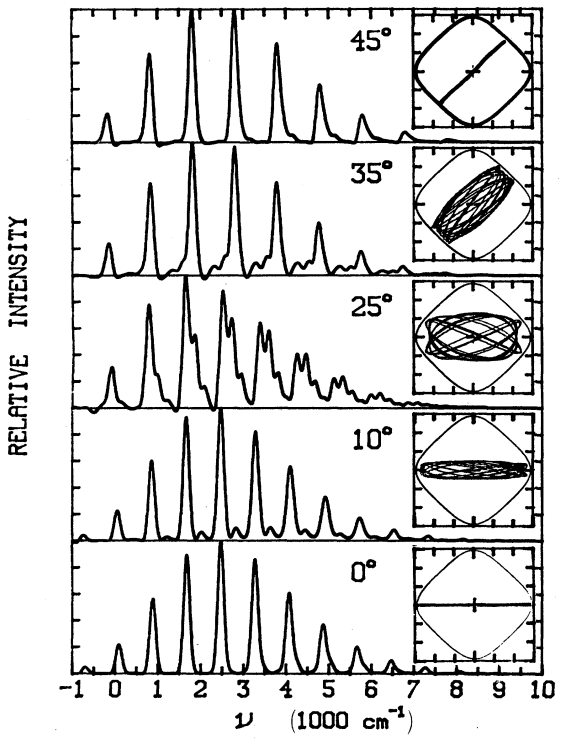

FIG. 7. With the term f_{xxzz}, which causes the two bending modes to become nondegenerate, set to a value of 0.047 87 mdyne, the effect of "aiming" the hydrogen atom along several directions in the bending mode subspace, by arranging for various momentum transfers, is shown.

Thus we can write

$$Y_{jj} = e^{-iE_0 t/\hbar} \langle 0 | e^{-i\mathbf{k}\cdot\hat{\mathbf{q}}_j} e^{i\hat{H}t/\hbar} e^{i\mathbf{k}\cdot\hat{\mathbf{q}}_j} | 0 \rangle \tag{5.8a}$$

$$= e^{-iE_0 t/\hbar} \langle \phi | e^{i\hat{H}t/\hbar} | \phi \rangle \tag{5.8b}$$

$$= e^{-iE_0 t/\hbar} \langle \phi(t) | \phi \rangle \ , \tag{5.8c}$$

where $|\phi(t)\rangle$ is the wave packet which evolves out of $|\phi\rangle$ under the action of the total Hamiltonian. The cross section is given by the Fourier transform of the correlation function (5.8c), which in turn is governed by the overlap between the initially boosted packet and the time-evolved version of that packet.

With this in mind, consider the qualitative changes seen in the panels of Fig. 7 as we go from top to bottom. In the 45° case, we can think of a wave packet initially at the origin, launched or boosted at a 45° angle due to the impulsive momentum transfer from the neutron. By symmetry of the potential, that direction is a periodic classical orbit. After the initial decay of the overlap $\langle \phi(t) | \phi \rangle$, there will be no significant overlap until the packet has returned to the starting position heading in the initial direction, i.e., at one period of the periodic motion. The recurrence at that time will be followed by others at multiples of the period, and the Fourier transform of this time dependence will be a series of peaks spaced at the frequency of the 45° periodic orbit. The envelope of the frequency domain peaks reflects the initial decay of the overlap. The rule of thumb is that the shorter-time features of the correlation function are reflected as the broader frequency features of the cross section. When the wave packet returns, it may have spread along the direction of motion perpendicular to the orbit, and this is reflected as continued reduction of the magnitude of the overlap at successive periods of the 45° orbit. This spreading is governed by the classical stability of nearby orbits, in accordance with the wave-packet dynamics described in Sec. III. This in turn is represented as broadening of the peaks. Eventually, the probability will return to the vicinity of the periodic orbit, which causes long-time recurrences responsible for resolving the peaks into finer structure. The fine-structure peaks must naturally occur at energy eigenvalues of the potential. The fine structure is not shown in Fig. 7, however, because of the resolution used and more importantly because the FGA was used, which prevented the Gaussian from spreading. [A fuller discussion of the spectral effects of various types of wave-packet dynamics can be found in Refs. 25 and 3(g).]

For scattering at 35°, 25°, etc., the orbits created by the momentum boost are now quasiperiodic instead of periodic, resulting in a slightly more complicated Lissajous pattern for the wave packets and thus for the correlation function. This pattern can be fully understood by running classical trajectories. They are shown in the insets in Fig. 7. It causes a multiple progression to appear in the Fourier space of the cross section. Finally at 0°, a periodic orbit is again relevant, but now the orbit has a different period; this is seen in Fig. 7 at the bottom panel as a closer spacing between the lines. The 25° trajectory covers the largest amount of classical phase space and also has the largest number of allowed energy band.

The possibility of exploring the potential energy surface with various momentum transfers is clearly revealed in the series of calculations shown in Figs. 4–7. In addition, since the potential energy surface is nontrivial and quite realistic, we have demonstrated the ability to handle situations beyond the usual impulse or harmonic regimes.

It is important to emphasize that by controlling the orientation of a crystal, scattering angle, energy of the beam, etc., it is possible to select the magnitude and direction of momentum boosts just as we have done theoretically here. We hope that the intuitive handle provided by the wave-packet picture will suggest new experiments designed to probe the potential energy surfaces and dynamics of molecules in crystals.

When are the wave-packet techniques a significant computational improvement over standard expressions? As far as we are aware, the wave packets are unique in their ability to handle anharmonic effects systematically. This makes application to liquid systems a distinct possibility.[4(g),12] On the other hand, it has long been established in the chemical physics literature that semiclassical wave packets are increasingly unreliable as propagation time increases on anharmonic potentials.[3,4] This translates into accurate low-resolution spectra and questionable high-resolution spectra, since long-time dynamics

are required for the latter.

Unlike many semiclassical techniques, wave packets make possible the systematic improvement of results by variational means. Methods for accomplishing the improvement of time-domain propagation have been given[3(b),4] and are still under development. This approach holds the promise of essentially exact neutron scattering spectra at the cost of increased computation effort.

The wave-packet picture of neutron scattering makes the classical-like dynamics of localized wave packets available as an intuitive and computational tool. On the computational side, we have just used the wave packets in a calculation that would have been inadequately described in any harmonic oscillator or separable approximation. The calculation would have been very difficult to perform using a basis set large enough to find all the eigenstates of the four-coupled-mode problem in the required energy regime. The inclusion of anharmonic lattice effects by direct use of a basis set would have been out of the question, but it is possible using time-dependent wave packets.

ACKNOWLEDGMENTS

This work was supported in part by National Science Foundation Grant No. CHE-8507138. We are grateful too for the hospitality and auspices of the T-12 group at Los Alamos National Laboratory, where this work began.

APPENDIX: ELECTRONIC SPECTROSCOPY ANALOGS TO NEUTRON SCATTERING

Recall that neutron scattering can be cast in a form involving a momentum-shifted Hamiltonian [Eq. (2.7)]. We can ease into the subject of electronic absorption spectra by means of another shifted Hamiltonian, where the shift is in position rather than momentum,

$$\hat{H}'_\rho = e^{i\rho\hat{p}}\hat{H}e^{-i\rho\hat{p}} = \hat{H}(\hat{p},\hat{q}+\rho) \ . \tag{A1}$$

In Fig. 8 we have shown a one-dimensional potential $\hat{V}$ and also $\hat{V}'$, which differs from $\hat{V}$ by a translation ρ and energy shift E_0. We have also shifted the energy of one of the potentials by E_0. This is not essential, but makes the situation more akin to electronic absorption between two Born-Oppenheimer potential surfaces. This energy shift merely displaces the energy spectrum of the transition by E_0. In addition to the effects included in Fig. 8, the general case of electronic absorption would involve a nonconstant transition-moment operator μ connecting $\hat{V}$ and $\hat{V}'$ and a change in the shape of $\hat{V}$ relative to $\hat{V}'$.

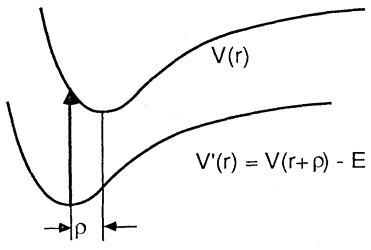

FIG. 8. Example of a shifted Hamiltonian. This case is a position shift affecting the potential V. An energy shift E_0 has been added.

The absorption spectrum for the shift Hamiltonian, which is the analog of the neutron scattering cross section, is proportional to the Fourier transform of

$$C_T(t) = \langle e^{i\hat{H}'_\rho t/\hbar} e^{-i\hat{H}t/\hbar} \rangle \tag{A2a}$$

$$= \langle e^{i\rho\hat{p}} e^{i\hat{H}t/\hbar} e^{-i\rho\hat{p}} e^{-i\hat{H}t/\hbar} \rangle \tag{A2b}$$

$$= \langle e^{i\rho\hat{p}} e^{-i\rho\hat{p}(t)} \rangle \tag{A2c}$$

$$= \langle e^{im\omega\rho\hat{q}} e^{-im\omega\rho\hat{q}(t)} \rangle \ . \tag{A2d}$$

The last version follows from the Heisenberg equations of motion for $\hat{p}$ and $\hat{q}$ for a harmonic oscillator, which are identical to the classical ones. Thus $\hat{p} = m\omega\hat{q}(t=\pi/2\omega)$, where $\hat{q}(t=\pi/2\omega)$ is the Heisenberg position at time $t=\pi/(2\omega)$. Then, since

$$\langle e^{im\omega\rho\hat{q}} e^{-im\omega\rho\hat{q}(t)} \rangle = \langle e^{im\omega\rho\hat{q}(\tau)} e^{-im\omega\rho\hat{q}(\tau+t)} \rangle \ ,$$

Eq. (A2d) follows. The temperature dependence is signified by a subscript T in $C_T(t)$. Equations (A2a)–(A2c) show the position-displaced case to be equivalent to an autocorrelation function involving the momentum (A2c). But Eq. (A2d) shows that is also a position autocorrelation function, directly equivalent to neutron scattering. An important practical application of this, within the harmonic approximation, is that the intensities of the lines shown in Fig. 4 can be obtained from tables of Franck-Condon factors, substituting momentum displacements on the usual position displacements.

It is intriguing that the position displacement, or more generally a mode displacement in the polyatomic or solid-state case, can be treated just as in neutron scattering. It suggests that the existing semiclassical techniques for neutron scattering can be carried over to solid-state and molecular spectroscopy, radiationless transitions, etc. We do not necessarily recommend this and do not pursue it, because $\hat{H}$ and $\hat{H}'$ generally differ by more than a shift. However, the strong similarities between the theories of neutron inelastic scattering and solid-state spectroscopy,[15] both in the harmonic approximation, have their origin in the equivalence just presented.

We go one step further into molecular electronic spectroscopy and now assume that $\hat{H}$ and $\hat{H}'$ differ in form because of a difference in the shape of the potentials $\hat{V}$ and $\hat{V}'$. Then the electronic-absorption spectrum is proportional to the Fourier transform of

$$C_T(t) = \langle \hat{\mu} e^{i\hat{H}'t/\hbar} \hat{\mu} e^{-i\hat{H}t/\hbar} \rangle \ , \tag{A3}$$

where we have included the possibility of a nonconstant transition moment operator $\hat{\mu}$. Now there is no way to proceed further to a simple Heisenberg autocorrelation function such as (A2c) and (A2d). Stranded without a suggestive Heisenberg autocorrelation function expression,

how are we to pass to a simple semiclassical approximation? A desperate attempt to write Eq. (A3) as

$$C_T(t)=\langle\hat{\mu}\hat{\mu}(t)\rangle \tag{A4}$$

with $\mu(t)$ given the appropriate definition fails, because $\mu(t)$ has a very odd and nonclassical behavior, since $\mu(t)$ is created out of two propagators that differ in essential ways and not just by a shift. The way out of this problem is to remain in the Schrödinger representation and evaluate the correlation function over the coherent-state Gaussian wave packets. This works nicely in the case of electronic spectroscopy.[25] Even for a spectroscopy which has a classical Heisenberg analog the Schrödinger representation discussed in this paper has considerable intuitive and computational advantage.

*Present address: Department of Theoretical Chemistry F11, University of Sydney NSW 2006, Australia.

[1]Leon Van Hove, Phys. Rev. **95**, 249 (1954).

[2]R. G. Gordon, Adv. Mag. Resonance **3**, 1 (1968).

[3](a) E. J. Heller, J. Chem. Phys. **62**, 1544 (1975); (b) **64**, 63 (1976); (c) M. J. Davis and E. J. Heller *ibid.* **71**, 3383 (1979); (d) E. J. Heller, Accounts of Chem. Research **14**, 368 (1981); (e) S. Y. Lee and E. J. Heller J. Chem. Phys. **76**, 3035 (1982); (f) E. J. Heller, *ibid.* **75**, 2923 (1981); (g) **68**, 3891 (1978); (h) M. Blanco and E. J. Heller *ibid.* **83**, 1149 (1985); (i) J. P. Bergsma, P. H. Berens, K. R. Wilson, D. R. Fredkin, and E. J. Heller *ibid.* **88**, 612 (1984); (j) J. R. Reimers, K. R. Wilson, E. J. Heller, and S. R. Langhoff, *ibid.* **82**, 5064 (1985); (k) G. Drolshagen and E. J. Heller, *ibid.* **79**, 2072 (1983); (l) G. Drolshagen and E. J. Heller, Chem. Phys. Lett. **104**, 129 (1984); (m) G. Drolshagen and E. J. Heller, Surf. Sci. **139**, 260 (1984); (n) G. Drolshagen and E. J. Heller, J. Chem. Phys. **82**, 226 (1985).

[4](a) M. F. Herman and E. Kluk, Chem. Phys. **91**, 27 (1984); (b) N. Corbin and K. Singer, Mol. Phys. **46**, 671 (1982); (c) B. Jackson and H. Metiu, J. Chem. Phys. **82**, 5707 (1985); (d) Judy Ozment, D. T. Chuljian, and J. Simons *ibid.* **82**, 4199 (1985); (e) R. T. Skodje and D. G. Truhlar, *ibid.* **80**, 3123 (1984); (f) R. D. Coalson and M. Karplus, Chem. Phys. Lett. **90**, 301 (1982); (g) D. V. Thirumalai, E. J. Bruskin, and B. J. Berne, J. Chem. Phys. **83**, 230 (1985).

[5]S. W. Lovesey, *The Theory of Neutron Scattering from Condensed Matter* (Oxford University Press, New York, 1984), Vol. I.

[6]J. R. Klauder and B. Stagerstam, *Coherent States* (World Scientific, Singapore, 1985).

[7]R. Littlejohn, Phys. Rep. **138**, 198 (1986).

[8]L. S. Schulman, *Techniques and Applications of Path Integration* (Wiley-Insterscience, New York, 1981).

[9]E. J. Heller, J. Chem. Phys. **65**, 4979 (1976).

[10]R. Coalson and M. Karplus, Chem. Phys. Lett. **90**, 301 (1982).

[11]W. H. Miller, Adv. Chem. Phys. **25**, 69 (1974).

[12](a) V. F. Sears, Phys. Rev. **185**, 200 (1969); (b) H. A. Gersch and P. N. Smith, Phys. Rev. A **4**, 281 (1971); (c) F. H. Stillinger and A. Rahman, *Molecular Dynamics Calculation of Neutron Inelastic Scattering from Water,* Proceedings of the 24th Annual Meeting of the Society of Chemical Physics, 1974 (unpublished), p. 479.

[13]M. Sargent III, M. O. Scully, and W. E. Lamb, *Laser Physics* (Addison-Wesley, Reading, Mass., 1974).

[14](a) A. Griffin and H. Jobic, J. Chem. Phys. **75**, 5940 (1981); (b) H. Jobic and R. E. Ghosh, *ibid.* **75**, 4025 (1981); (c) A. C. Zemach and R. J. Glauber, Phys. Rev. **101**, 118 (1956).

[15](a) K.-S. Rebane, *Impurity Spectra of Solids* (Plenum, New York, 1970); (b) R. Kubo and Y. Toyozowa, Prog. Theor. Phys. **13**, 2 (1955).

[16](a) M. Rosenbaum and P. F. Zweifel, Phys. Rev. **137**, 271 (1965); (b) J. E. Moyal. Proc. Cambridge Philos. Soc. **45**, 99 (1949).

[17]E. J. Heller, J. Chem. Phys. **65**, 1289 (1976).

[18](a) S. Carter, I. M. Mills, and J. N. Murrell, J. Mol. Spec. **81**, 110 (1980); (b) G. Strey and I. M. Mills, Mol. Phys. **26**, 129 (1973); (c) A. R. Hoy, I. M. Mills, and G. Strey, Mol Phys. **24**, 1265 (1972).

[19](a) G. Simons, R. G. Parr, and J. M. Finlan, J. Chem. Phys. **59**, 3229 (1973); (b) J. M. Finlan and G. Simons, J. Mol. Spec. **57**, 1 (1975); (c) G. Simons, J. Chem. Phys. **61**, 369 (1974).

[20]G. D. Carney, L. A. Curtiss, and S. R. Langhoff, J. Mol. Spec. **61**, 371 (1976).

[21]R. W. Munn and R. J. Newham, Chem. Phys. **14**, 309 (1976).

[22](a) S. A. Rice and M. Sceats, J. Chem. Phys. **71**, 973 (1979); (b) S. A. Rice and M. Sceats, J. Chem. Phys. **72**, 3236 (1980).

[23]J. R. Reimers and R. O. Watts, Chem. Phys. Lett. **94**, 222 (1983).

[24]R. E. Hoffman and E. F. Horning, J. Chem. Phys. **17**, 1163 (1949).

[25](a) E. J. Heller, in *Potential Energy Surfaces and Dynamics Calculations,* edited by D. G. Truhlar (Plenum, New York, 1981); (b) E. J. Heller, Acc. Chem. Res. **14**, 368 (1981).